Journal of Applied Mechanics and Technical Physics, Vol. 37, No. 6, 1996

MECHANISMS OF SPALLING OF METALS IN THE FAST SPACE-HEATING REGIME IN SUBMICROSECOND AND SUBMILLIMICROSECOND RANGES OF DURABILITY

E. K. Bonyushkin, B. L. Glushak, N. I. Zavada, S. A. Novikov, L. A. Platonova, N. I. Sel'chenkova, I. R. Trunin, A. Ya. Uchaev, and N. A. Yukina

UDC 620.17:539.2:539.12.04

It is known [1, 2] that fast heating of materials by pulsed flows of penetrating radiation gives rise to compressive stresses whose amplitude in the solid-phase region is proportional to the concentration of the absorbed energy.

The time lag of the absorbing medium causes a motion in the form of compression waves (or shock waves) and expansion waves. The interaction of two counter waves of the latter type gives rise to tensile stresses in the material with duration $\tau_t \sim \Delta/c$ (Δ is the thickness of the heated layer and c is the speed of sound). The amplitude of these stresses depends, in the general case, on the absorbed energy, the heating rate (the rate of energy supply), the distribution of the absorbed energy in mass, and the physicomechanical properties of the medium. The appearance of tensile stresses produces conditions for the development of failure. When critical amplitude–time characteristics of the impulse of tensile stresses are reached in a cross section of the sample, failure of the normal separation (spalling) type occurs in it.

Investigation of the dynamic effects caused by fast heating of a material is very important for applications, because the capabilities of modern high-energy pulsed facilities are largely determined by the mechanical strength of elements, units, and constructions.

The thermal-shock method used in studies of failure allows a considerable extension of the range of the material states studied as compared with conventional methods (shock-wave and explosion loadings [3, 4]). Thus, the results of these investigations provide new information on the behavior of specific materials and are of independent importance for the physics of failure, in particular, in developing models of failure under high-speed deformation that fit the process well.

Materials can be fast heated by impulsive penetrating radiation (in particular, by a nuclear explosion [5]) and by pulsed beams of charged particles [3, 6–10]. The spalling of some solid media (colored ice and polyvinyl chloride plastic) under absorption of the laser-radiation energy is considered in [1, 8, 10]. The spalling of some metals upon fast space heating by high-current electron beams is described in [3, 5, 7–9, 10].

Sources of impulsive radiation allow one to investigate the behavior of materials in the region of extreme loading parameters and over a wide range of initial temperatures.

In studies of the failure of metals under laboratory conditions, high-current accelerators of relativistic electrons are the most widely used sources of pulsed pressure. Use of these accelerators offers unique possibilities and new avenues of attack on the problem of failure of solid bodies in the submicrosecond range of durability for the following acting parameters: rate of energy supply dE/dt of up to 10^{11} J/(g · sec), concentration of the absorbed energy $E \sim 1$–10^3 J/g, initial temperatures $T_0 = 4K$–$0.8T_{\text{melt}}$, and electron energy $\mathcal{E}_e \sim 1$–10 MeV. The experimental methods developed to date in combination with mathematical modeling make it possible to obtain a detailed picture of dynamic failure.

The present paper reports new results of experimental studies and numerical simulation. Both the new data and previous data are analyzed and generalized.

Institute of Experimental Physics, Sarov 607190. Translated from Prikladnaya Mekhanika i Tekhnicheskaya Fizika, Vol. 37, No. 6, pp. 105–115, November–December, 1996. Original article submitted July 21, 1995.

 0021-8944/96/3706-0862 $15.00

1. We consider some aspects of stress dynamics in a continuous medium under fast space heating. A great portion of the radiant energy penetrating into the medium is absorbed by the electron subsystem. During the electron–ion relaxation time τ_{ei} (for metals $\tau_{ei} \sim 10^{-11}$ sec), the excitation energy of the electron subsystem is transferred to the ion subsystem. If the energy is supplied fast enough, compressive stress arises in the body, because the potential well is asymmetrical and the time of establishment of heat equilibrium is finite. The further development of the process is associated with the wave motion of the continuous medium. The character of this motion depends on specific boundary conditions, the medium's geometry, and heating conditions. The final result of the mechanical reaction of the solid body, i.e., failure or preservation of continuity, is determined by the amplitude–time characteristics of tensile stresses and the tensile strength of the medium.

Instantaneous uniform-in-mass heating is a theoretical model concept that is not realized in practice. For the subsequent analysis of experimental results, we distinguish the main calculated features of the behavior of a material under fast nonuniform heating. Generally, when heat conduction for monochromatic radiation is ignored, the absorbed-energy distribution $E(m,t)$ in time and in the mass of a flat sample under irradiation is described by the expression

$$E(m,t) = E_0 f(m) \int_0^t \mathcal{E}(t)dt,$$

where $\mathcal{E}(t)$ is the radiation intensity; $f(m)$ is the mass-distribution function of the absorbed energy [the functions $\mathcal{E}(t)$ and $f(m)$ are normalized to unit energy]; and E_0 is the energy absorbed in the sample, which is actually close to the energy of the beam incident normally to its surface.

We found the stress fields in the tested metallic samples by numerical simulation solving a system of equations for one-dimensional motion. For this, we used a finite-difference scheme in Lagrangian variables and introduced linear-quadratic artificial viscosity. The absorbing medium is considered elastoplastic with a constant yield limit. The spherical component of the stress tensor is taken in the form of the Mie–Grüneisen equations of state $P = P_c + P_T = P_c + \Gamma\rho c_V(T - T_0)$, where Γ is a constant value of the Grüneisen coefficient and $P_c = \rho_0 c_0^2/n(\delta^n - 1)$ is the potential component of pressure, where $\delta = \rho/\rho_0$ is the relative compression.

Let us analyze separately the effect of the nonuniformity of the temperature-field distribution [the function $f(m)$] and the heating time or the rate of energy supply [the function $\mathcal{E}(t)$ or $T(t)$] on the stress field using copper as an example. We specify several typical model temperature fields (Fig. 1a, curves 1–4 correspond to different absorbed-energy profiles) in such a manner that the total energy absorbed by the sample is constant, ignoring the difference in the actual functions $f(m)$, which is insignificant for various materials and sources of space heating. The following parameters of the equation of state for copper are used in the calculations: $\rho_0 = 8.93$ g/cm^3, $c_0 = 3.95$ km/sec, $n = 4.26$, $\Gamma = 2.0$, yield limit $Y = 0.23$ GPa, and Poisson coefficient $\nu = 0.34$.

In the instantaneous-heating regime, the initial stress profiles $\sigma_0(x)$ obviously represent the corresponding distribution profiles $E(x)$, because $\sigma_0(x) = \Gamma\rho_0 E(x)$ and $E(x) = E(m/\rho)$. Figure 1b shows the relative positions of the calculated stress fields across the thickness of the copper sample at $t = 5 \cdot 10^{-8}$ sec in the instantaneous-heating regime ($t_i = 0$). The curve numbers correspond to the distributions $E(m)$ in Fig. 1a. The data show a relatively weak effect of the temperature-field profile on the stress field both in the compression wave and in the expansion wave. For moderate deviations of the distribution $E(x)$ from uniformity, the corresponding stress fields differ little from each other. The situation changes if these deviations are large. For a triangular distribution, the form of the expansion wave changes significantly, and the position of the amplitude maximum of tensile stresses is shifted toward weaker heating of the material (curve 4 in Fig. 1b).

When heating is sufficiently uniform in mass, spalling takes place in the middle plane of the sample or in the vicinity of this plane, as follows from an experiment on flat samples with free boundaries. The time dependences of the normal stress σ_x in the middle plane of the sample (Fig. 1b) show that in this case the amplitude–time characteristics of tensile stresses are close to each other when the difference in the values of the function $f(m)$ is insignificant. The tension σ_x turns out to be smaller compared with the maximum

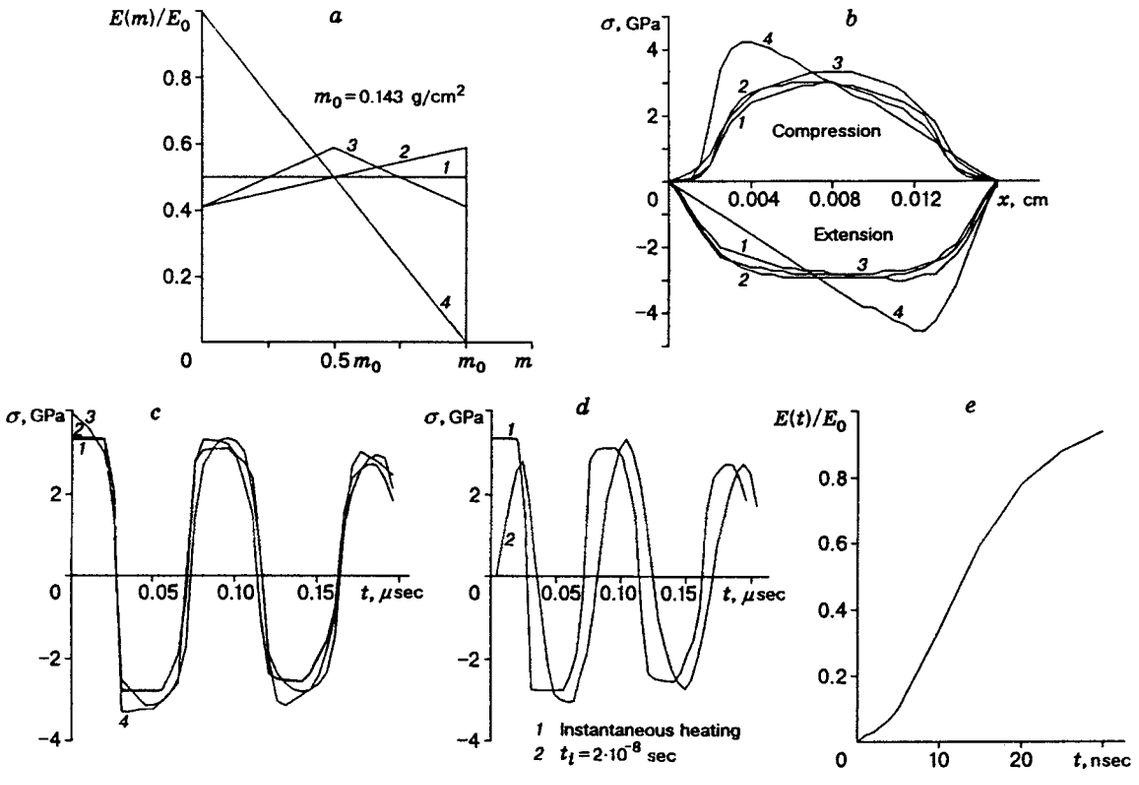

Fig. 1

amplitude in the compression wave, and this is a consequence of the dependence of the sound velocity on the relative compression, in accordance with the equation of state adopted in the calculation model. For the same reason, the time of action of tensile stresses τ_t increases somewhat in comparison with the acoustic approximation.

We now briefly consider the effect of the finite time of heating on the results of numerical simulation. For this, the necessary calculations are performed for a time dependence of radiation intensity that is fairly close to the actual incident electron beam intensity. The radiation intensity $\mathcal{E}(t)$ is assumed to be constant over the time interval $t_i = 20 \cdot 10^{-9}$ sec. Thus, the heating is considered a linear function of time. It should be noted that over this time interval most of the total energy (approximately 90%) of the electron beam is absorbed in the irradiated target, i.e., the model dependence of $\mathcal{E}(t)$ is an acceptable approximation.

The model-calculation results (Fig. 1d) show that the amplitude and duration of the tensile stresses in the middle plane of the sample are practically independent of time for heating times of from $t = 0$ to $t \approx \Delta/2c$, where Δ is the length of the heated layer for the absorbed-energy profile (curve 1 in Fig. 1a). At the same time, the effect of finiteness of the heating time manifests itself in the regions on both sides of the middle plane. This is associated with the expansion-wave propagation from the free surfaces into these regions before the termination of irradiation. In accordance with the calculation results, the maximum amplitude and shape of the tensile-stress pulse for model profiles 1–3 of the absorbed energy $E(m,t)$ (Fig. 1a) differ little from each other for both instantaneous heating $[E(m)]$ and heating for $t_i = 20$ nsec $[E(t)]$ [Fig. 1d, which gives the model dependence of the radiation intensity $\mathcal{E}(t)$]. This indicates that, for the heat-loading regimes considered, the tensile-stress pulse is mainly determined by the absorbed-energy concentration averaged over the mass of the sample. In the subsequent discussion, the calculation results are used to interpret experimental data.

2. In the experiments, fast space heating of metals was realized by a pulsed flow of relativistic electrons with maximum energy $\mathcal{E}_e \approx 3$ MeV generated by an RIUS-5 accelerator [3, 7–10]. The distribution of

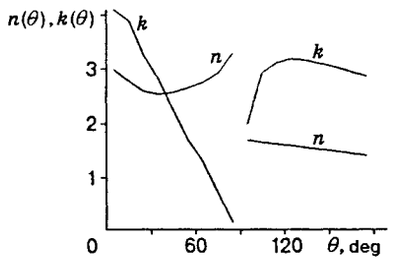

Fig. 2

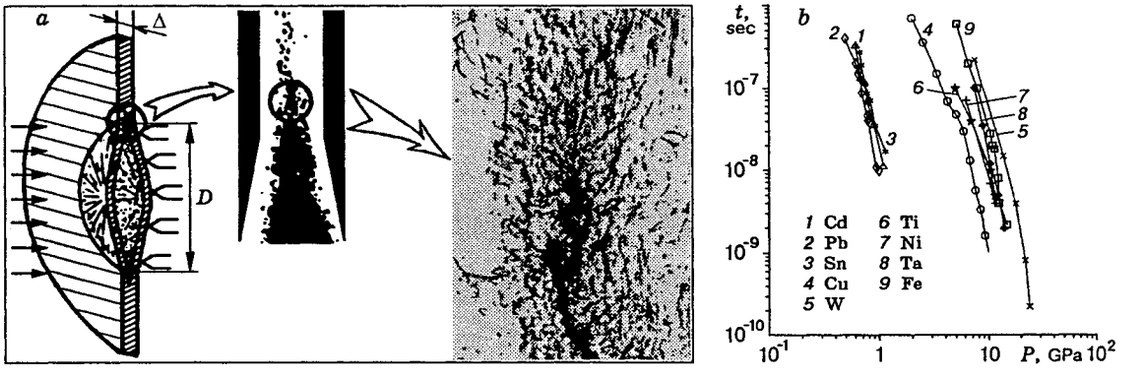

Fig. 3

the electron-beam-energy fluence over a spot, which characterizes the absorbed-energy distribution over the irradiated surface of the target, is found by a noncontact method. This method is based on the relationship between the braking radiation generated upon electron absorption [11] and the electron-fluence profile. In this case, the image of the braking radiation on a converter was constructed by means of a camera obscura with the subsequent transfer of the visible image to a photomatrix [11]. A series of calculations on electron-energy transfer was carried out by the Monte Carlo technique [12] to substantiate the method. The angular distribution $W_\gamma(\theta)$ of the energy output of braking radiation is given by

$$W_\gamma(\theta) = k(\theta) I \mathcal{E}_e^{n(\theta)}, \tag{2.1}$$

where I is the electron-beam current, and $k(\theta)$ and $n(\theta)$ are coefficients that depend on the observation angle θ, and the thickness and type of the target (θ is measured from the system axis coinciding with the electron flow direction).

Figure 2 gives the coefficients $n(\theta)$ and $k(\theta)$ for a tantalum target with $\Delta = 1$ mm in the energy range of 0.5 MeV $\leqslant \mathcal{E}_e \leqslant$ 3 MeV for a normal incidence of electrons on the target. A comparison of expressions (2.1) and $W_e = I\mathcal{E}_e$ shows that information on the beam-fluence profile can be obtained from the braking radiation only in the particular case where $\mathcal{E}_e$ = const. In the general case, the relationship is varying and depends on $\mathcal{E}_e$: $W_e = W_\gamma / k\mathcal{E}_e^{n-1}$.

When the braking radiation is recorded on the frontal side of the sample (θ = 90–180°), this relationship is weaker than on the opposite side (θ = 0–90°). In the first case, the fluences can be determined by selection of the composition and thickness of the converter using a single image.

In the second case (θ = 0–90°), we have to construct two images with two different converters; the Monte Carlo method is used to determine local values of $\mathcal{E}_e$ and optimize the composition of the converters for both variants. The pressure-pulse profile is measured simultaneously by manganin sensors located on the back side of the irradiated sample, which is "tightened up" by a material with a smaller acoustic stiffness.

Figure 3a shows the spalling scheme and a microsection of a copper sample with a thickness of Δ =

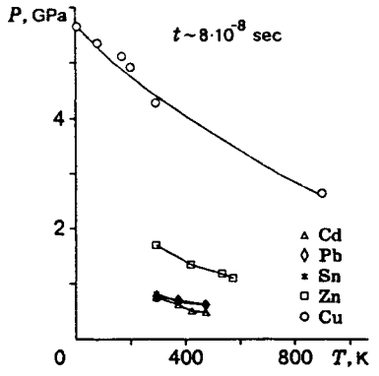

Fig. 4

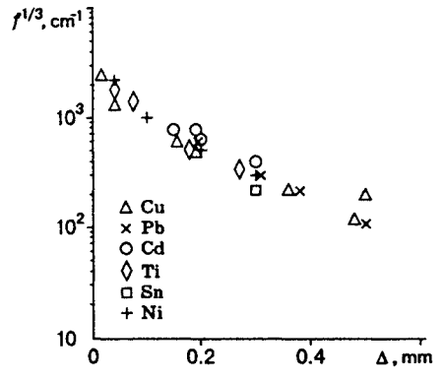

Fig. 5

$5 \cdot 10^{-5}$ m. Figure 3b presents the results of investigations of the time dependences of dynamic failure. The curves in the Fig. 3b show the boundaries above which there is the region of failure (the method for determining the boundaries can be found in [3, 7, 9, 10]). The data indicate that the negative stresses σ (concentration of the absorbed energy E) have a progressing effect on the rate of the process. The irradiated samples were preheated by the radiant-heat flux from a heater and cooled to the boiling point of helium to determine the temperature dependence of the critical fracture stresses. Thus, the range of initial temperatures $T_0 = 4K$–T_{melt} can be considered. Figure 4 shows temperature curves (isochrones, $t \sim 8 \cdot 10^{-8}$ sec) for the dynamic failure process under thermal shock. The data (Fig. 4) demonstrate that dynamic failure is described by the three-parametric function $\sigma_{\text{cr}} = \sigma(T, t)$ (see also [3, 9, 10]). According to the data, the absorbed energy E_{cr} is substantially less than the energy parameters of the lattice. This indicates that the elementary acts of the destruction reaction are of a thermofluctuation nature, and, hence, follows the progressing effect of the absolute temperature and negative stresses on the dynamic failure of the tested materials. The methods described make it possible to find specific patterns for each material.

Determination of the leading stage and general mechanisms of the process is of special importance. The basic approach involves separating the set of phenomena in space and time and "freezing" the process at a required stage. Information on the failure process after its termination can be obtained by fractographic studies of microsections of the fracture surface and of adjacent planes that are perpendicular and parallel to the fracture plane using an interactive system for image analysis.

An image of the surface formed is transmitted to a monitor by means of a microscope working in the reflected-light regime and a telecamera. The information contained in the image matrix is represented by blackening levels varying over the field (the number of levels at a point is 256). The concave part of the "mountain relief" of the fracture surface is a structural measurable element [3, 10].

The fractographic studies of the fracture surface show that the average dimensions of roughnesses of the spall surface $\langle D \rangle$ differ little for various metals over a wide time range and initial-temperature range [3, 9, 10, 13, 14] $T_0 \sim 4K$–$0.8T_{\text{melt}}$. Figure 5 gives the ultimate density of the fracture centers f on the fracture surface as a function of the sample thickness Δ for the critical value of the absorbed energy E_{cr}. This suggests that the ultimate density of the fracture centers in various metal samples (their durability being the same) differs little for the critical absorbed energy causing failure.

The method of finding the spectral size distribution of the fracture centers from fractographic data for microsections that are parallel and perpendicular to the fracture surface is used to determine the mechanisms of formation of a cascade of these centers at different stages of the process (Fig. 6a and 6b). The images of the perpendicular microsections are cut into separate bands parallel to the fracture surface. The number and spectral size distribution of the fracture centers are determined in each band. The time t of tensile-stress action is different in each band and increases as a band "approaches" the fracture surface under uniform heating. The microsections parallel to the fracture surface were also processed. The number and spectral distribution of

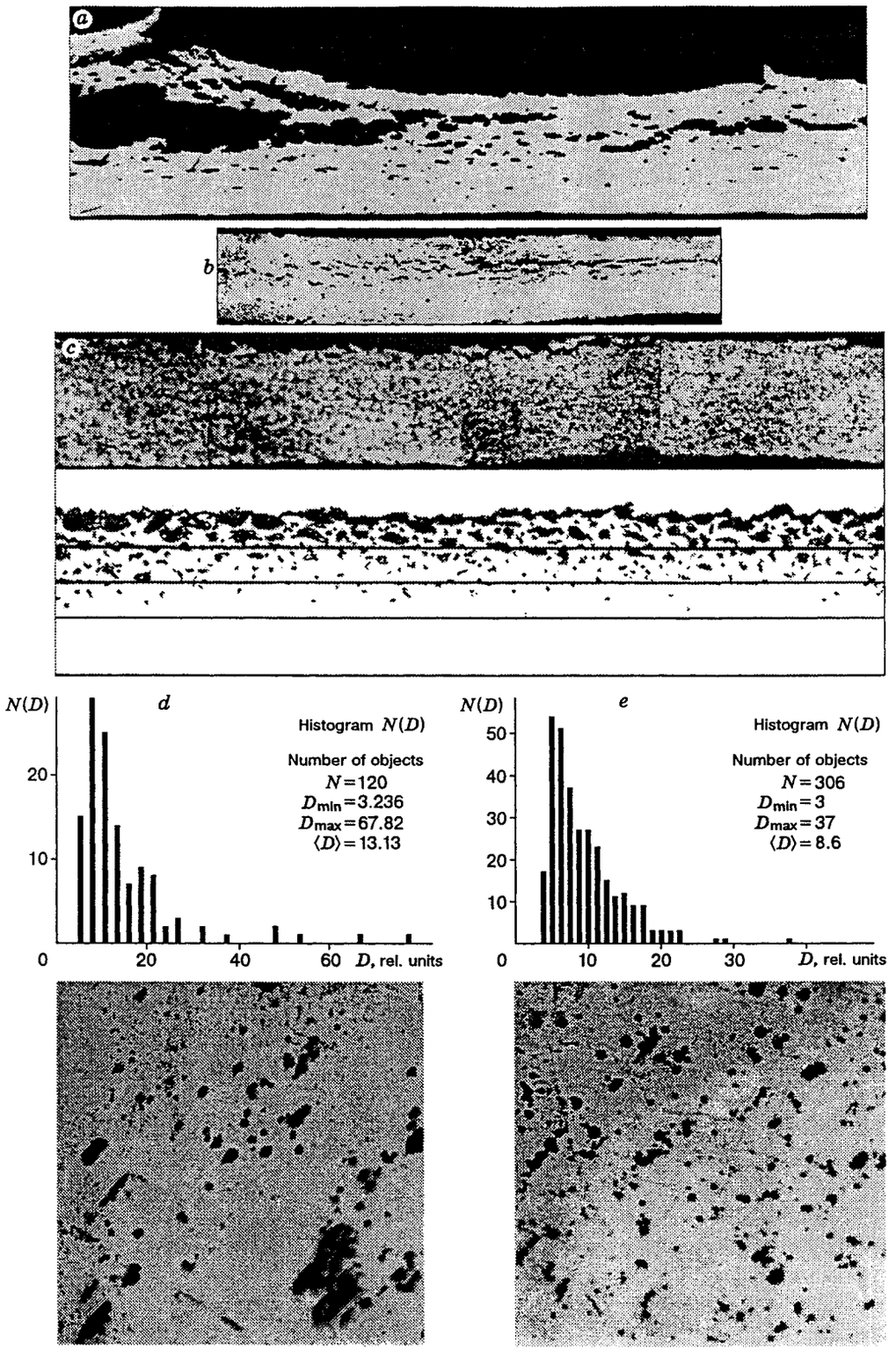
a
b
c
d
N(D)
Histogram N(D)
Number of objects
N=120
Dmin=3.236
Dmax=67.82
⟨D⟩=13.13
D, rel. units
e
N(D)
Histogram N(D)
Number of objects
N=306
Dmin=3
Dmax=37
⟨D⟩=8.6
D, rel. units

Fig. 6

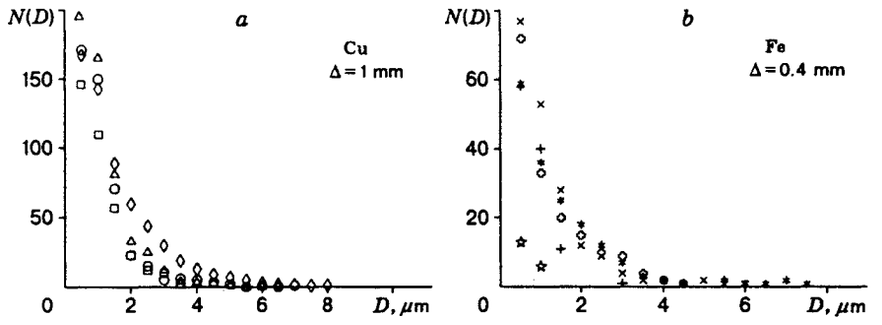

Fig. 7

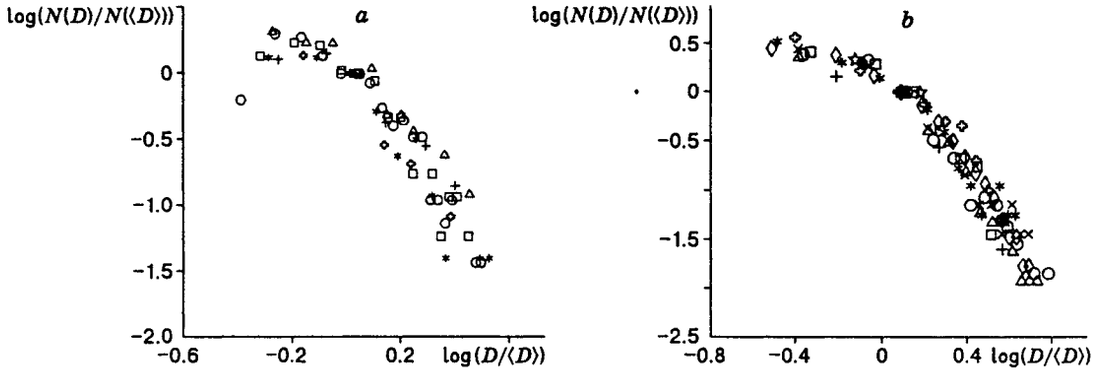

Fig. 8

the fracture centers are found for each microsection. The processing scheme is given in Fig. 6c. Figure 6d and 6e shows microsections that are parallel to the fracture surface and a histogram for the spectral distribution of the fracture centers (Fig. 6d shows the data for brass, $\Delta = 4 \cdot 10^{-4}$ m, and the distance from the fracture surface is $l = 5 \cdot 10^{-5}$ m; Fig. 6e refers to copper, $\Delta = 10^{-3}$ m, and $l = 2.5 \cdot 10^{-4}$ m).

Figure 7 gives the distribution $N(D)$ in microsections that are perpendicular to the fracture surface for a copper sample, with $\Delta = 10^{-3}$ m (a) and iron sample with $\Delta = 4 \cdot 10^{-4}$ m (b). Figure 8a and 8b shows the data in the coordinates $\log D/\langle D\rangle$ versus $\log N(D)/N(\langle D\rangle)$. The results presented can be approximated by a single curve, and, hence, the size distribution of the fracture centers at different stages of the process can be obtained by a similarity transformation. The cascade of the fracture centers grows as a self-similar geometrical object during the failure process. This indicates that dynamic failure proceeds by a single predominant mechanism of development involving the accumulation and growth of the fracture centers, which determines most of the durability. Thus, the geometrical self-similarity of the cascade of the fracture centers, which is described by the expression $N(D) \sim D^{-\alpha}$, is an important property governing the kinetics of the process.

The power distribution $N(D)$ is typical of fractals [15]. During the growth of a fractal cluster, only its sizes vary, but the dimensionless distribution $N(D) \sim N(\langle D\rangle)(D/\langle D\rangle)^{-\alpha}$ does not change (Fig. 8). This suggests that the kinetics of accumulation of the fracture centers in the indicated ranges of t, σ, and T can be described within the framework of a self-similar approximation [15].

It seems that the observed general features of the accumulation and growth of the fracture centers cannot but affect the macrofeatures of the dynamic failure process.

The study of the fractograms of microsections shows the occurrence of zones of the material's plastic motion (similar to convection or turbulence). The elements of these zones move in accordance with the scheme of translation plus rotation. This leads to the loss of stability of the crystal lattice. Figure 9 shows plastic-flow regions occurring near a growing fracture center in a copper sample ($\Delta = 3.7 \cdot 10^{-4}$ m) at different loading

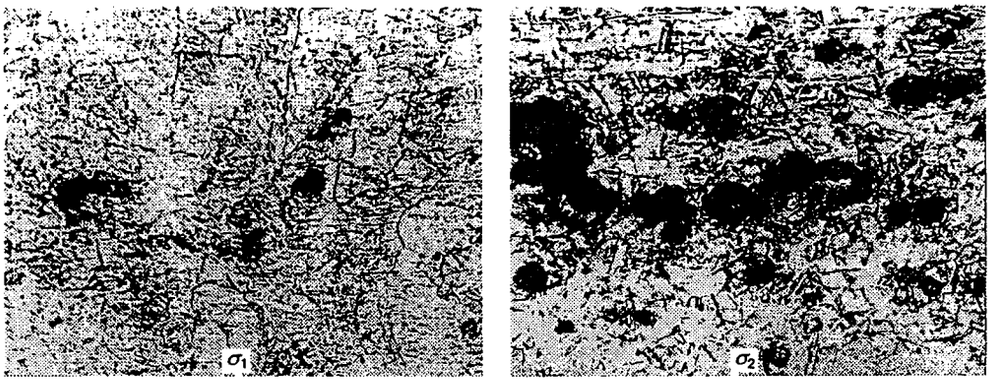

Fig. 9

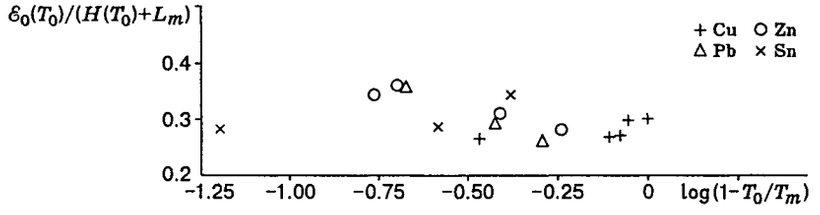

Fig. 10

levels ($\sigma_1 < \sigma_2$). A structural-energy analogy in the behavior of the metal–external-action system to which thermal and mechanical energy is delivered is noted in the modern literature [16, 17]. This leads in both cases to a disruption of the long-range order, i.e., to the loss of stability of the lattice. Detection of plastic-motion zones in the regions of appearance and growth of the fracture centers makes it possible to study the mechanisms of dynamic failure by representing the temperature dependences for some materials [for close values of durability (Fig. 10)] in the coordinates $\log(1 - T_0/T_{\text{melt}})$ versus $\mathcal{E}(T_0)/[H(T_0) + L_m]$, where $H(T_0)$ is the enthalpy H for T_0 and L_m is the heat of melting. It is seen from Fig. 10 that, for all the metals investigated, the ratio of $\mathcal{E}_{\text{cr}}(T_0)$ to $[H(T_0) + L_m]$ has close values and is practically independent of $(1 - T_0/T_{\text{melt}})$. This allows prediction of the temperature dependence of materials under thermal shock.

Note that combination of calculation-theoretical and experimental approaches described in the paper is now a general method for studying the failure process. In particular, this makes it possible to determine the actual durability for complex types of failure such as multiple spalling [3, 7].

Systematization of the results obtained in studying the properties of some elements and determination of the general mechanisms of dynamic failure enable one to predict the behavior of unstudied materials under extreme conditions.

REFERENCES

1. A. A. Kalmykov, I. V. Nemchinov, and A. I. Petrukhin, "An experimental investigation of scattering of an instantaneously heated material and appearance of a pulse at energy concentrations smaller than the heat of evaporation," *Zh. Prikl. Mekh. Tekh. Fiz.*, **6**, 3–13 (1966).
2. L. W. Morland, "Generation of thermoelastic stress waves by impulsive electromagnetic radiation," *AIAA J.*, **6**, No. 6, 1063–1066 (1968).
3. A. Ya. Uchayev, E. K. Bonyushkin, S. A. Novikov, and N. I. Zavada, *The Spalling of Metals in the Regime of Fast Space Heating. Review* [in Russian], TsNIIatominform, Moscow (1991).

4. B. L. Glushak, V. F. Kuropatenko, and S. A. Novikov, *Investigation of the Strength of Materials under Dynamic Loading* [in Russian], Nauka, Novosibirsk (1992).
5. A. I. Pavlovskii, E. K. Bonyushkin, V. V. Varaksin, et al., "An investigation of a pulsed chemical HF-laser with gamma radiation pumping," *Dokl. Ross. Akad. Nauk*, **331**, No. 3, 229–331 (1993).
6. J. L. Perkin, E. Morris, and D. W. Large, "The spalling of aluminum with a pulsed electron beam," *J. Phys. D, Appl. Phys.*, **4**, 974–984 (1974).
7. A. Ya. Uchayev, S. A. Novikov, V. A. Tsukerman, et al., "The spalling of tungsten in the fast space-heating regime," *Dokl. Akad. Nauk SSSR*, **310**, No. 3, 611–614 (1990).
8. V. A. Sviridov, B. L. Glushak, and S. A. Novikov, "An experimental investigation of the behavior of cadmium and polyvinyl chloride plastic under pulsed heating by laser radiation," in: *Proc. 1st All-Union Conf. on Detonation*, Chernogolovka (1979), pp. 152–155.
9. A. I. Pavlovskii, E. K. Bonyushkin, A. Ya. Uchayev, et al., "The temperature–time mechanisms of the dynamic failure of some metals in the fast space-heating regime," *Dokl. Ross. Akad. Nauk*, **317**, No. 6, 1376–1379 (1991).
10. E. K. Bonyushkin, I. V. Zhukov, N. I. Zavada, et al., "The spalling of constructional materials in the fast space-heating regime and under explosive loading," in: *Questions of Atomic Science and Engineering*, Ser: *Pulsed Reactors and Simple Critical Assemblies*, No. 1 (1988), pp. 53–61.
11. V. M. Gorbachev, N. I. Zavada, V. N. Korolyov, et al., "A system for investigating the configuration of an electron beam using the braking radiation on a target," *Prib. Tekh. Éksp.*, No. 5, 163–166 (1992).
12. E. N. Donskoi, "The ELISA technique and program. Solution of the problems of simultaneous transfer of gamma radiations, electrons, and positrons by the Monte Carlo method," in: *Questions of Atomic Science and Engineering*, Ser: *Mathematical Modeling of Physical Processes*, No. 1 (1993), pp. 3–6.
13. A. I. Pavlovskii, E. K. Bonyushkin, N. I. Zavada, et al., "On the determination of the height of the potential barrier of an elementary destructive reaction in the dynamic failure process," in: *Zababakhin Scientific Lectures*, Abstracts of Chelyabinsk-70 (1992), p. 175.
14. A. I. Pavlovskii, E. K. Bonyushkin, N. I. Zavada, et al., "The kinetics of nucleation in the process of dynamic failure by thermal shock," *ibid.*, p. 176.
15. G. I. Barenblatt, *Similarity, Self-Similarity, Intermediate Asymptotics* [in Russian], Gidrometeoizdat, Leningrad (1982).
16. V. V. Fyodorov, *The Thermodynamic Aspects of the Strength and Failure of Solids* [in Russian], Fan, Tashkent (1979).
17. V. E. Panin, V. A. Likhachev, and Yu. V. Grinyayev, *Structural Levels of Deformation of Solid Bodies* [in Russian], Nauka, Novosibirsk (1985).